Applied Physics A (2022) 128:370
https://doi.org/10.1007/s00339-022-05462-8

Applied Physics A
Materials Science & Processing

Upconversion luminescence enhancement of the composite films by coupling local surface plasmon effect and photonic crystals effect

Haifang Zhou[1,2] · Xuehua Weng[1] · Jiaxin Zou[1] · Yunfeng Lai[1,3] · Jinling Yu[1] · Shuying Cheng[1]

Received: 20 October 2021 / Accepted: 4 March 2022 / Published online: 4 April 2022

Abstract
Noble metal surface plasmon resonance or photonic crystals (PCs) effect is a novel and effective method for improving upconversion luminescence (UCL). UCL can be effected by the size, thickness of the noble metal film and the photonic band gap (PBG) of the PCs. So it is important to improve UCL by coupling surface plasmons resonance (SPR) with PCs effect. In this work, the PCs/Ag/UC composite films were fabricated to improve the upconversion emission of $NaGdF_4$:Er^{3+}/Yb^{3+}/Al^{3+} nanocrystals, and the influence of the Ag layer thickness on spectral properties was investigated. Studies reveal that the Ag layer thickness and morphology have a major impact on the Ag nanoparticles (NPs) plasma resonance and UCL intensity of $NaGdF_4$:Er^{3+}/Yb^{3+}/Al^{3+} nanocrystals for PCs/Ag/UC composite films. The highest enhancement factors of the red and green emissions were found to be 43 and 42 under 980 nm excitation, respectively. That is attributed to the coupling effect of the Ag NPs local SPR and PCs Bragg reflection, the local electromagnetic field enhancement produced by the excitation wavelength overlapping with the photonic band gap and strong plasmon resonance band overlapping with emission wavelength.

Keywords Upconversion enhancement · PCs/Ag/UC composite films · $NaGdF_4$:Er^{3+}/Yb^{3+}/Al^{3+} nanocrystals · Local electromagnetic field enhancement

1 Introduction

Upconversion nanoparticles (UCNPs) doped with rare earth (RE) ions have unique physical feature such as high chemical stability, narrow emission band, large anti-Stokes shifts [1, 2], and great application potential in harvesting infrared light for solar cells, biological fluorescence imaging and sensing, white light-emitting diodes, optical thermometry and etc. [3–6]. However, weak emission intensity of UCNPs due to the low luminous efficiency and small absorption cross-section limits their application. Some methods have been applied to improve the efficiency and brightness of UCL, such as searching for more efficient hosts, tuning the types and concentrations of the doping ions, designing core–shell structures, coupling with noble metal nanostructures and photonic crystals [7–11]. Plasmon structure has been proved to be an efficient tool to enhance UCL [12]. Light impinging on a metal NPs can resonate with the metal NPs surface plasmon, that is localized surface plasmon resonance (LSPR), producing a dipolar field outside the particle. That produces local electromagnetic field (LEMF) strength near the surface of the metal NPs and UCNPs, if the resonant wavelength can overlap with the absorption/emission wavelength of the UCNPs, fluorescence emission intensity greatly enhances [13], and the UCL depends strongly on the distance between UCNPs and metal NPs, the type and particle size of the metal [14]. Photonic crystals with periodic dielectric structure have some properties such as photonic band gap, photonic localization, and so on [15, 16]. The light at the edges of the photonic band gap (PGB) can be propagated with the reducing group velocity due to Bragg diffraction, and local density of optical states (LDOS) become increase on the surface of PCs [17]. At the edges of the PGB, the LDOS has a maximum, and a high LEMF enhancement, which can lead

✉ Haifang Zhou
zhhafa@163.com

[1] School of Physics and Information Engineering, and Institute of Micro-Nano Devices & Solar Cells, Fuzhou University, Fuzhou 350108, People's Republic of China

[2] Jiangsu Collaborative Innovation Center of Photovoltaic Science and Engineering, Changzhou 213164, Jiangsu Province, People's Republic of China

[3] Fujian Science & Technology Innovation Laboratory for Optoelectronic Information of China, Fuzhou 350108, People's Republic of China

to a higher absorption of the emitter. The PCs structure has been proved to be an effective method to enhance UCL, if the excitation or emission band of UCNPs can couple with the PBG, UCL is improved due to the increase of the optical transition rate or the spontaneous emission rate, which is related to the LDOS [18]. In addition, the dielectric PCs structures cause less quenching than the plasmonic structures. So the coupling of the photonic crystals and the surface plasmon effect is an efficient tool for UCL fluorescence enhancement, and it can enhance UCL up to 3 orders [19].

$NaGdF_4$ with a lower phonon energy has been shown good UC performance [20]. Recently, the UCL improvement for $NaGdF_4$-based NPs has been mainly obtained by the means of ions doping, core–shell structure, size control, morphology and surface control, etc. [21–24], there is few report on coupling the plasmon resonance effect and the PCs effect for UCL enhancement. For the plasmon effect, it have been found that the LEMF depends on the configuration and dielectric properties of the plasmonic nanostructure such as the distance between emitter and plasma, size and morphology of the metal NPs, and periodic structure [19]. The absorption, energy transfer and the donor decay, are important for the overall enhancement of upconversion, and the absorption cross section, decay rates and energy transfer rates can be affected by photonic and plasmonic nanostructures [18, 19]. The absorption and emission can be improved by increasing the LEMF at the position of the emitter [17]. The UCL intensity of Er^{3+}/Yb^{3+}-codoped materials can be enhanced by the means of metal ions doping [6, 21], in this work, $NaGdF_4:Er^{3+}/Yb^{3+}$ doped with Al^{3+} ions NPs were synthesized, we fabricated a PCs/Ag/UC composite films to further enhance UCL of $NaGdF_4:Er^{3+}/Yb^{3+}/Al^{3+}$ nanocrystals by coupling Ag NPs plasmon effect and PCs Effects. The PCs were fabricated on glass substrates using polystyrene microspheres for coupling the excitation field, Ag NPs were deposited on the surface of the PCs by a thermal evaporation for coupling the emission field due to plasmon resonance, then $NaGdF_4:Er^{3+}/Yb^{3+}/Al^{3+}$ nanocrystals were coated on the surfaces of the PCs/Ag structure, the effect of Ag film thickness on the UCL of PCs/Ag/UC composite films was systematically studied, and the corresponding UC enhancement mechanism was analyzed.

2 Experimental

2.1 Synthesis of upconversion nanocrystals

All reactants and solvents are analytically pure, and can be used without further purification. $RE(CH_3COO)_3$(RE = Gd, Yb, Er) with high purity (99.99%) were purchased from Shanghai Chemical Co., ethylenediamine tetraacetic acid (EDTA, reagent grade, ≥ 99%), NaF (reagent grade, ≥ 99%) and $AlCl_3$ (reagent grade, ≥ 99%) were purchased from Fuzhou Lianyou Experimental Instruments. $NaGdF_4:Er^{3+}/Yb^{3+}/Al^{3+}$ nanocrystals were synthesized by a solvothermal method. Firstly, 3 mmol of EDTA was dissolved in 50-mL deionized water at 50 ℃ under stirring for 30 min. Subsequently 16 mmol of NaF was dissolved in the above solution under stirring for 30 min, then the 2 mmol mixture of $Gd(CH_3COO)_3$, $Yb(CH_3COO)_3$, $Er(CH_3COO)_3$, and $AlCl_3$ with corresponding mole ratios ($Gd^{3+}:Yb^{3+}:Er^{3+}:Al^{3+}$ = 63:20:2:15) was dripped into the above solution. After vigorously stirring at 50℃ for 2 h, the colloidal solution was transferred into a 100 mL teflon autoclave, sealed, and maintained at 200 ℃ for 12 h. The solution was then allowed to naturally cool to room temperature, and the nanocrystals were separated by centrifugation, washed with ethanol and deionized water several times for removing any possible remnants, and then dried in vacuum at 60 ℃ for 24 h. The samples were then annealed in a nitrogen atmosphere at 250 ℃ for 2 h.

2.2 Fabrication of the PCs/Ag/ UC films

Figure 1 illustrates the fabrication process of the PCs/Ag/UC composite films. Firstly, The PCs layer was fabricated on the glass substrates by the vertical self-assembly method. The glass substrate was soaked in hydrogen peroxide and sulfuric acid with the corresponding volume ratio (3:7) for 8 h for the sake of hydrophilicity. Then, the glass substrate was vertically positioned into the a mixed solution of deionized water and ethanol with a molar ratio of 1:3, containing 0.1wt% monodisperse polystyrene microspheres with an average diameter of 400 nm, and baked in a oven at 55 °C for 48 h. After the solvent evaporated, the PCs were baked at 80 °C for 30 min to increase its adhesion to the glass, and form periodic photonic crystal layer. Secondly, the Ag films with thickness of 5, 8, 10 and 12 nm were deposited on the surface of PCs by the thermal evaporation, respectively. The deposited rate was controlled at 0.12 Å/s in the vacuum of 9×10^{-5} Pa. Lastly, 0.2 g $NaGdF_4:Er^{3+}/Yb^{3+}/Al^{3+}$ nanocrystals were dissolved in 4 mL ethanol and

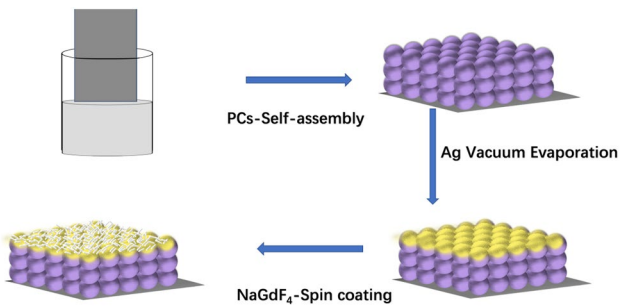

Fig. 1 The fabrication process of PCs/Ag/UC films

oscillated by ultrasonic wave for 30 min. Then a drop of UC nanocrystals colloidal solution was spin-coated several times on the surface of the Ag film at a speed of 2000 rpm. Then the polymethyl methacrylate solution was spin-coated to cover the surface of the UC to form a PCs/Ag/ UC films.

2.3 Measurements

The PCs/Ag/UC films samples were examined and characterized. The morphology of PCs films, Ag NPs and $NaGdF_4$:Yb^{3+}/Er^{3+}/Al^{3+} nanocrystals were observed by dual-beam field emission scanning electron microscope (FESEM, Helios G4 CX). The diffuse reflectance, transmittance and absorbance spectra of PCs/Ag films were acquired by the ultraviolet–visible-near-infrared spectrophotometer (Agilent Cary5000). The UC emission spectra were recorded by the spectrophotometer (Edinburgh Instrument FLSP920), combined with lifetime and steady-state fluorescence spectrometer under the excitation of 980 nm laser with an excitation power density of 50 mW/mm^2. All performance characterizations achieved at room temperature.

3 Result and discussion

The SEM images of PCs, PCs/Ag, $NaGdF_4$:Yb^{3+}/Er^{3+}/Al^{3+} are presented in (Fig. 2a–f). It can be seen in (Fig. 2a) that the PCs are densely packed in close face-centered cubic (FCC). After depositing Ag particles on the surface of PCs, the Ag NPs size becomes larger, and the longitudinal size of the particles become longer with the depositing time increase, the surface morphology on the top of the PCs varies from discrete (Fig. 2b–c) to partial continuous (Fig. 2d–e). The nano rod-like $NaGdF_4$:Er^{3+}/Yb^{3+}/Al^{3+} distributed on the surface of the PCs/Ag hybrid structure are observed, in (Fig. 2f), the cross-section image shows that continuous UCNPs films (~ 700 nm) are formed on the surface of PCs/Ag, indicating that a dense layer of UC nanocrystals formed on the surface of the PCs/Ag hybrid structure. EDS was used to measure the elemental components of the PCs/Ag/UC, the main element peaks of Na, F, Gd, Yb, Al and Ag are observed in the EDS pattern (Fig. 2f), which confirms Er^{3+}/Yb^{3+} and Al^{3+} ions were successfully doped into $NaGdF_4$ nanocrystals.

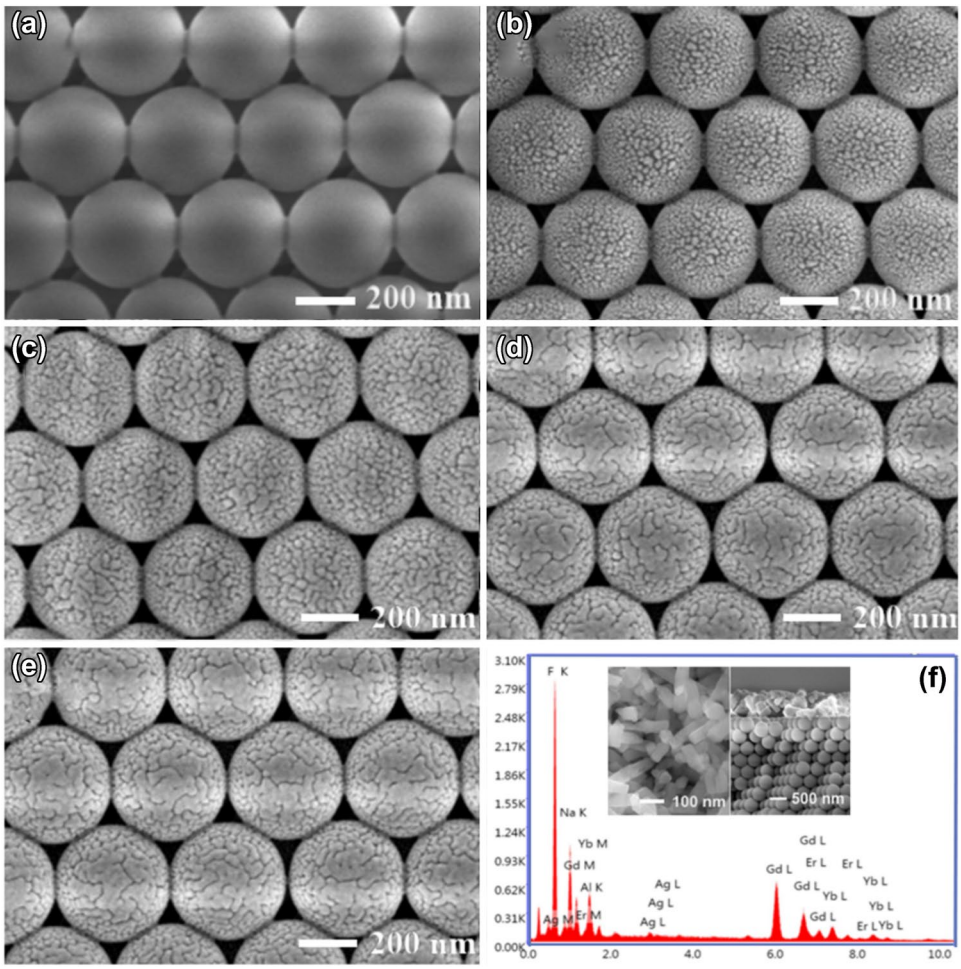

Fig. 2 SEM images of (**a**) PCs, and PCs with the different thickness of Ag: (**b**) 5 nm, (**c**) 8 nm, (**d**) 10 nm, (**e**) 12 nm, (**f**) EDS pattern for $NaGdF_4$:Yb^{3+}/Er^{3+}/Al^{3+} nanoparticles decorated on the PCs/Ag hybrid structure surface. The inset of the SEM of $NaGdF_4$:Yb^{3+}/Er^{3+}/Al^{3+} nanocrystals and the corresponding cross-section image of hybrid film

The PBG of PCs with the ordered FCC structure can be expressed using Bragg's law [25, 26]:

$$\lambda = 1.633D(n_{eff}^2 - \sin^2\theta)^{1/2} \quad (1)$$

$$n_{eff}^2 = n_{ps}^2 f_{ps} + n_{air}^2(1 - f_{ps}) \quad (2)$$

In these equations, λ is the position of the photonic band gap, θ represents the angle of incidence, D and f_{PS} denote the diameter of the microspheres and the volume fraction of the microspheres (f_{PS} is 74% for the PCs), respectively. n_{eff}, n_{air} and n_{ps} represent refractive index of the PCs, air and microspheres, respectively. To study the influence of Ag on the optical properties of PCs/Ag, the transmittance, diffuse reflectance and absorbance were measured, as shown in Fig. 3. It can be seen from the transmittance spectra that the PBG of the PCs locates around 978 nm in the (Fig. 3a), that is agreement with the value of 952 nm obtained from the Eq. (1). After depositing Ag NPs on the surface of the PCs, the central locations of the PBG remain unchanged, indicating that deposition of Ag NPs on the PCs surfaces has no influence on the position of the PBG. However, the PBG of the PCs/Ag films becomes shallower and broader after the introduction of the Ag NPs, that is attributed to the presence of an absorbing layer, leading to the ordered degree decrease of the PCs. The prominent diffuse reflection peak is located at 978 nm for the PCs in (Fig. 3b), with the increase of the Ag film thickness, the red-shift of reflection peak for PCs/Ag films is increased from 18 to 54 nm, and the reflection intensity is decreased, that is ascribe to the absorption of the Ag film of different thickness and surface effect of the PCs. In addition, with the increasing of Ag film thinckness, the two resonance peaks of about 515 nm and 967 nm hav e been observed in the (Fig. 3b) except for the sample with 5 nm thickness Ag, which do not show a distinct plasmon peak at around 967 nm due to the high surface scattering of electrons for small nanoparticles [27]. The lower wavelength peak due to the transverse polarization mode remains nearly at fixed locations around 515 nm which is found coincident with plasmon band of the spherical particles [17]. The higher peak owing to the longitudinal polarization mode becomes stronger and broader, and has a little red-shift with the size increase of Ag nanoparticles. The red-shift arises from a reduction of the depolarization field due to retardation effects [27]. and the result is consistent with that of the literature [28]. Be compared with PCs, the absorption is enhanced after depositing silver on the surface of PCs, the strongest absorption intensity at around 500 nm is observed for the samples with the thickness of 8 nm Ag, but the strongest absorption intensity at round 978 nm is obtained for the samples with the 12 nm Ag. The enhanced absorption at around 500 nm is attributed to the LSPR and the PCs effect, which overlapped with the emission band of the UCNPs can enhance UCL. However, the enhanced absorption of Ag NPs at 978 nm can lead to the improvement of nonradiative transitions instead of the radiative transitions enhancement of UCNPs. As strong scattering of PCs/Ag composite films is helpful to absorption transition of the emitters under the excitation wavelength, the thickness of Ag film is very important for coupling plasma effect and photonic crystal effect to enhance UCL.

UC emission spectra from PCs/Ag/UC composite structures with different Ag film thicknesses have been obtained under excitation wavelength of 980 nm, as shown in (Fig. 4a). It can be seen that the emission spectra have one strong and two weak emission peaks at 655 nm, 541 nm and 521 nm, respectively. They are corresponding to the $^4F_{9/2} \rightarrow {}^4I_{15/2}$, $^4S_{3/2} \rightarrow {}^4I_{15/2}$ and $^2H_{11/2} \rightarrow {}^4I_{15/2}$ electron transitions of Er^{3+} ions, respectively. The UC mechanism of the Er^{3+}/Yb^{3+}-codoped materials induced by near infrared light generally belongs to the two photon excitation process. Figure 4b shows the energy level diagram of Er^{3+} and Yb^{3+} ions to elaborate the energy transfer processes, UC emission mechanism of the $NaGdF_4$:Er^{3+}/Yb^{3+}nanocrystals is similar to that of $KLaF_4$:Er^{3+}/ Yb^{3+} and BiOF:Er^{3+}/Yb^{3+} nanoparticles [29, 30]. As the thickness of Ag film increases from 0 to 12 nm, luminescence enhancement due to coupling plasmon resonance and PCs effect for the PCs/

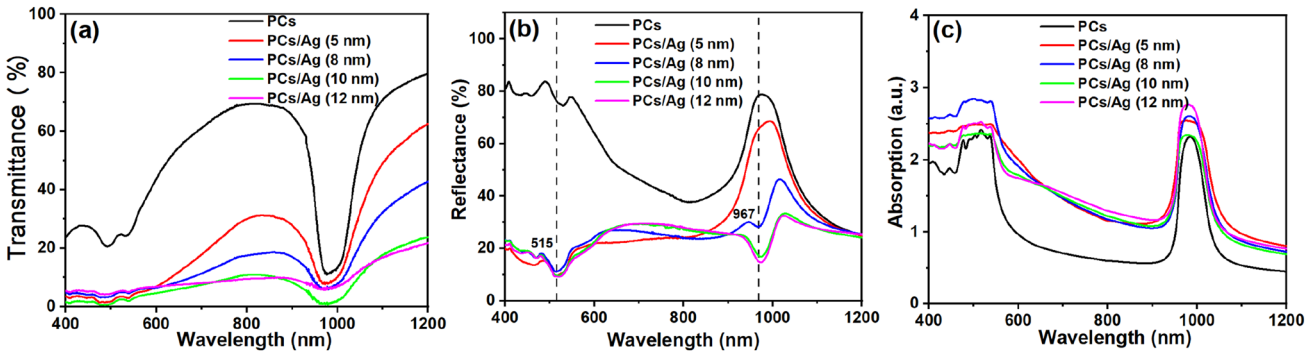

Fig. 3 The spectra of (**a**) transmittance, (**b**) reflectance spectra and (**c**) absorbance for the PCs/Ag films with a different Ag film thicknesses

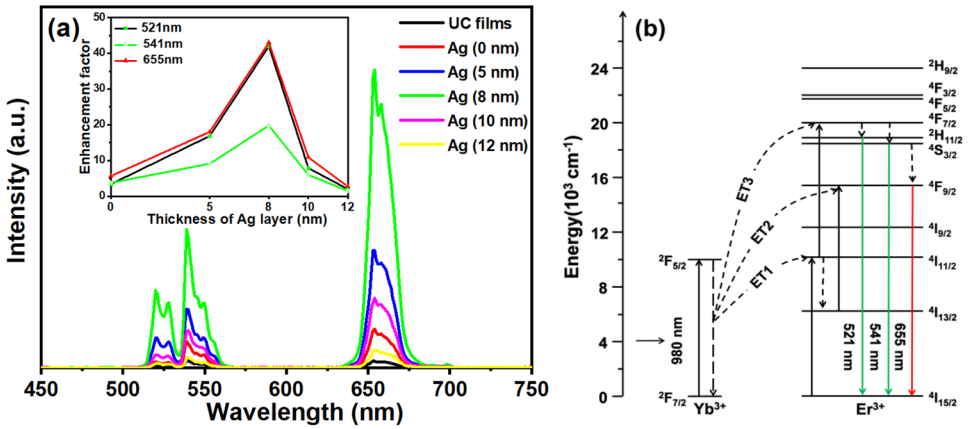

Fig. 4 **a** The UCL spectra of PCs/Ag/UC films under 980 nm excitation at room temperature. The inset shows the PL enhancement factor of green and red emission as a function of Ag film at different thickness. **b** Energy levels of Yb^{3+} and Er^{3+} ions relevant to the energy-transfer upconversion process under 980 nm excitation

Ag/UC films is observed. The fluorescence intensity reaches a maximum for the sample with thickness of 8 nm Ag. The inset shows that the maximum enhancement factors for the green emission of 541 nm and 521 nm, red emission are achieved to be 20, 42 and 43, respectively.

The luminescence enhancement for PCs/UC sample is attributed to the excitation enhancement due to the high photonic DOS at the PGB (Fig. 3a), which increases the LEMF and leads to a higher absorption of the UCNPs. The absorption cross section enhanced by the LEMF can be express as [31]:

$$\sigma_a = c\mu_0\omega \mathrm{Im}(\alpha)\frac{|n_d \cdot E(r)|^2}{|E_0|^2} \tag{3}$$

where c and μ_0 are the velocity of light and permeability in a vacuum, respectively, ω is the frequency of absorption light. E_0 and $E(r)$ are the incident and the local field at the position of the emitter, respectively. n_d is the unit vector along the induced dipole moment direction, α is the polarizability, and $\mathrm{Im}(\alpha)$ is imaginary part of α which is determined by the transition matrix element and only related to the electronic wavefunctions [18]. So the absorption cross section enhancement for the PCs/UC sample is ascribe to $|E/E_0|^2$ which relates to LDOS, and the enhancement factors due to the excited absorption for the green emission of 541 nm and 521 nm, red emission are achieved to be 3.8, 3.4 and 5.7, respectively.

For ellipsoidal mental nanoparticles with principal axes a, b, and c, the polarizability (α) along the principal axes ($i=1$, 2, 3) can be expressed as [27]:

$$\alpha(\omega) = \frac{4\pi abc}{3}\frac{\varepsilon(\omega)-\varepsilon_m}{\varepsilon_m + L_i(\varepsilon(\omega)-\varepsilon_m)}, \sum_{i=1}^{3} L_i = 1 \tag{4}$$

where, $\varepsilon(\omega)$ (ε_m) is the dielectric permittivity of the metal (dielectric). The dielectric permittivity of Ag NPs is modeled with a Drude model [32]:

$$\varepsilon(\omega) = 5.45 - \frac{0.73\omega_p^2}{\omega^2 - i8.35\omega \times 10^{13}} \tag{5}$$

where ω_p represents the plasma frequency of the Ag bulk metal. An ellipsoidal particle is considered, and the depolarization factors L_i is be taken into account the different polarization along the principal axes. When the module of complex denominator in $\alpha(\omega)$ is a minimum (Fröhlich condition), the resonance occurs, and the polarizability α is resonantly enhanced. For spherical particles, $L_1=L_2=L_3=1/3$, and only one resonance condition (a short-axis mode) occurs. For spheroidal particles, $L_1=L_2$. the plasmon resonance thus splits into a strongly redshifted long-axis mode polarization in addition to a short-axis mode (Fig. 3b). The LSPR of neighboring Ag NPs for separation distances couples through near-field interactions, enabling the NPs to act as an electric dipole, consequence of the resonantly enhanced polarization α is a concomitant enhancement in absorbing and scattering electromagnetic fields. The localization field in small gaps due to the geometric effect and multiple photon scattering on rough surfaces contribute to this high field enhancement in nanometer-sized volumes [27].

It can be seen from Eqs. (4) and (Fig. 3b) that strength and resonant wavelength of the dipolar plasmon resonance are related to the size of Ag NPs. So the higher luminescence enhancement for PCs/Ag/UC samples is attributed to the excitation and emission enhancement due to the coupling effect between LSPR and PCs. It can be seen from the reflectance spectra and absorption spectra in (Fig. 3b and c) the LSPR emerges at around 515 nm and 967 nm after depositing Ag NPs on the surface of PCs, the resonance wavelength overlaps with the 521 nm green emission and 980 nm excitation absorption of UCNPs, the LEMF around Ag NPs and UCNPs is greatly enhanced, that can enhance the absorption cross section and the emitting radiative rate of UCNPs, resulting in fluorescence intensity enhancement [12]. Both the absorption and emission processes, which

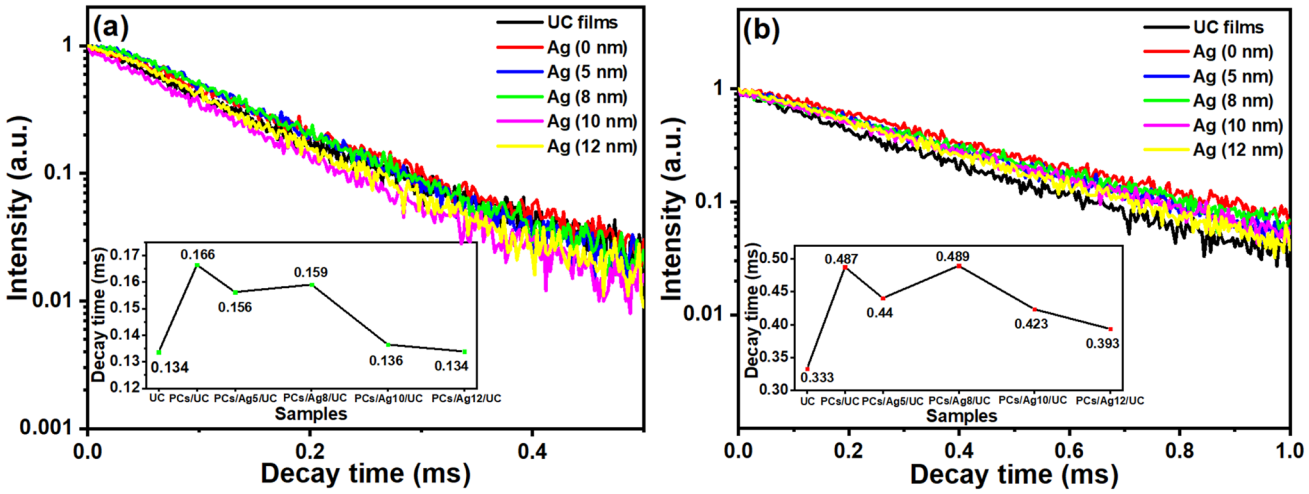

Fig. 5 Decay profiles of (**a**) $^4S_{3/2} \rightarrow {}^4I_{15/2}$ and (**b**) $^4F_{9/2} \rightarrow {}^4I_{15/2}$ transition for UC and PCs/Ag/UC films. The inset shows the decay time of samples

involve the exchange of photons through interaction of the emitter with the LEMF. The emission transition rate can be expressed by Fermi's golden rule [17, 33]:

$$\Gamma_{\text{rad}} = \frac{2\pi\omega}{3\varepsilon_0 V}|\mu_{g^*,e}|^2\rho_d(\hbar\omega) \tag{6}$$

Where V is the volume in which the electromagnetic (EM) field is confined, ε_0 the vacuum permittivity, $\mu_{g*,e}$ *is* the dipolar moment of the transition (electron transition from the excited state $|e\rangle$ to low energy state $|g^*\rangle$), and is related to the selection rules of the electronic system, $\omega = (E_e - E_{g*})/\hbar$. $\rho_d(\hbar\omega)$ is the photonic density of states (DOS), and it is determined by the boundary conditions of the EM environment. So the emission transition rate can be accomplished by increasing the EM field.

The maximum upconversion enhancement for the sample with the thickness of 8 nm Ag film is mainly ascribed to the increasing emission transition rate due to the increasing LEMF of the emitter, which is mainly caused by the stronger broad plasma resonance effect in the range of 475–540 nm in addition to the PCs effect (Fig. 3c). However the introduction of the plasmonic resonance can increase the nonradiative decay rates and result in fluorescence quenching, and the scattering of LSPR for the excitation light induces the increase of the excitation rate due to the LEMF enhancements [34]. The typical formation of LSPR critically depends on the configuration of the nanostructure. For a flat continual metal surface, the effective excitation of LSPR can hardly be realized because of the mismatch in the wave vector momentum condition [35]. So UCL for PCs/Ag/UC is decreased due to the partial continuous Ag surface, even the nonradiative decay due to the strong absorption of the Ag film exceeds the enhanced excitation effect for the sample with 12 nm Ag film, producing the weaker UCL than that of the PCs/UC sample.

We measured the time behavior of the $^4S_{3/2} \rightarrow {}^4I_{15/2}$ and $^4F_{9/2} \rightarrow {}^4I_{15/2}$ transitions for the composite films with the different Ag thickness under the 980 nm excitation. Figure 5 shows that the $^4S_{3/2} \rightarrow {}^4I_{15/2}$ and $^4F_{9/2} \rightarrow {}^4I_{15/2}$ transitions can be well fitted to a single exponential function. The inset in (Fig. 5a) shows the decay lifetime for $^4S_{3/2} \rightarrow {}^4I_{15/2}$ transition is found to firstly increase from 0.134 ms to 0.166 ms, and then decrease to 0.134 ms with increasing the Ag film thickness. There is a small variation of the decay rates for the samples with the Ag NPs and PCs. Because the optical transition ($^4S_{3/2} \rightarrow {}^4I_{15/2}$) involves only a two-step population regime and thus has the lowest sensitivity to the excitation influence [36], the coupling contributes a little to the whole dynamic process. Figure 5b shows the decay lifetime of the $^4F_{9/2} \rightarrow {}^4I_{15/2}$ transition, and it firstly increases from 0.333 to 0.487 ms, and then decreases from 0.489 to 0.393 ms with increasing the Ag film thickness, this trend is similar to the $^4S_{3/2} \rightarrow {}^4I_{15/2}$ transition, the longer lifetime of $^4F_{9/2}$ states is found in the PCs/UC and PCs/Ag/UC samples. For the PCs/UC sample, the longer radiative decay time is attributed to the decrease of the decay rate of the intermediate energy levels of $^2F_{5/2}$ and $^4I_{11/2}$ for Yb^{3+} and Er^{3+}, due to the high photonic DOS. Surface plasma resonance can change three rate constants of the decay rate of the emitting level, the excitation and the intermediate levels for the PCs/Ag/UC samples [31]. In the case of excitation matched plasmonic nanostructures, the plasmon would influence both the radiative and nonradiative decay rates of the intermediate levels. So the longer decay time for the sample with 8 nm Ag film is attributed to the decrease of the decay rate of the intermediate energy levels rather than the emitting level, since the intermediate level decay is affected more severely [31]. With

the decreasing of distance d between UCNPs and the surface of Ag NPs due to more continuous silver surface, the nonradiative decay rate of the electric dipole transitions become faster, it is the $1/d^3$ distance dependence of the nonradiative decay rate near the metal surface [37], leading to the increase of the total decay rate for the samples with 10 nm and 12 nm Ag film.

4 Conclusions

In a word, a structure of PCs/Ag/UC films was fabricated on a glass substrate, the UC emission of the $NaGdF_4:Er^{3+}/Yb^{3+}/Al^{3+}$ nanocrystals deposited on the surface of the PCs/Ag films was investigated in the case of the variety of silver thickness. The UC emission strongly depends on the coupling effect of the Ag NPs LSPR and PCs Bragg reflection, and the thickness and morphology of the Ag NPs in PCs/Ag/UC films play an important role in the UC emission enhancement. The strongest red and green emission intensities were obtained for the sample with an 8 nm thickness Ag layer. That is attribute to the excitation wavelength overlapping with the photonic band gap and strongest plasmon resonance band overlapping with emission wavelength. However, quenching effect rather than enhancement effect was occurred for a more continuous Ag surface due to the nonradiative decay exceeding the enhanced emission. The small variation of the decay rates and the lower enhancement in upconversion luminescence for the $^4S_{3/2} \rightarrow {}^4I_{15/2}$ transition are attributed to the lower sensitivity to the excitation influence, the variety of the decay time for $^4F_{9/2} \rightarrow {}^4I_{15/2}$ transitions is mainly ascribed to the decay rate of the intermediate energy levels.

Acknowledgements This work was supported by the National Nature Sciences Fundation of China (No. 62074036), the Nature Sciences Fundation of Fujian Province (No. 2021J01582 and 2019J01218), Fujian Science & Technology Innovation Laboratory for Optoelectronic Information of China (No.2021ZR145).

Declaration

Conflict of interest The authors declare that they have no conflict of interest.

References

1. Y. Ji, W. Xu, D. Li, D. Zhou, X. Chen, N. Ding, J. Li, N. Wang, X. Bai, H. Song, Semiconductor plasmon enhanced monolayer upconversion nanoparticles for high performance narrowband near-infrared photodetection. Nano Energy **61**(6), 211–220 (2019)
2. K. Park, M. Park, H.S. Jang, J.H. Park, J. Kim, Y. Cho, I.K. Han, D. Byun, H. Ko, Highly secure plasmonic encryption keys combined with upconversion luminescence nanocrystals. Adv. Funct. Mater. **28**(21), 1800369 (2018)
3. S.S. Mathilde, Z. Hu, D.O.L. Karmel, H. Xiang, G. Patrick, M. Michel, B. Laurent, A. Lionel, Z. Chen, Microscopic evidence of upconversion-induced near-infrared light harvest in hybrid perovskite solar cells. Acs Appl. Energy Mater. **1**(8), 3537–3543 (2018)
4. S. Xu, Y. Yu, Y. Gao, Y. Zhang, X. Li, J. Zhang, Y. Wang, B. Chen, Mesoporous silica coating $NaYF_4$:Yb, Er@NaY_F4 upconversion nanoparticles loaded with ruthenium(II) complex nanoparticles: Fluorometric sensing and cellular imaging of temperature by upconversion and of oxygen by downconversion. Microchim. Acta. **185**(10), 454–464 (2018)
5. P. Du, W. Ran, Y. Hou, L. Luo, W. Li, Eu^{3+}activated $NaGdF_4$ nanorods for near-ultraviolet light-triggered indoor illumination. ACS Appl. Nano Mater. **2**(7), 4275–4285 (2019)
6. J. Tang, P. Du, W. Li, L. Luo, Boosted thermometric performance in NaGdF4:Er3+/Yb3+ upconverting nanorods by Fe3+ ions doping for contactless nanothermometer based on thermally and nonthermally coupled levels. J Lumin. **224**, 117296 (2020)
7. J. Hu, R. Wang, R. Fan, F. Wang, H. Xiong, Z. Huang, L. Liu, H. Fu, Nanocomposites of Au nanorods and core-shell $NaGdF_4$:Yb^{3+}, E^{r3}+@NaY_F4 upconversion nanoparticles for temperature sensing. ACS Appl. Nano Mater. **3**(10), 9679–9685 (2020)
8. Q. Wang, C. Zhang, M. Liu, H. Ma, X. Wang, The synthesis of newly developed $Li_{(1-x-y)}Na_xK_yYF_4$:Yb^{3+}/$Er^{3+}$and its excellent upconversion properties. Opt. Mater. **108**, 110164–110170 (2020)
9. J. Xie, W. Hu, D. Tian, Y. Wei, E. Liang, Selective growth and upconversion photoluminescence of Y-based fluorides: from $NaYF_4$:Yb/Er to YF_3:Yb/Er crystals. Nanotechnology **31**(50), 9 (2020)
10. Z. Zhang, C. Huang, N. Li, J. Wei, Fabrication of multicolor Janus microbeads based on photonic crystals and upconversion nanoparticles. J. Colloid Interf. Sci. **592**(14), 249–258 (2021)
11. T. Gao, X. Zhu, X. Wu, B. Zhang, H. Liu, Selectively manipulating upconversion emission channels with tunable biological photonic crystals. J. Phys. Chem. C. **225**(1), 732–739 (2021)
12. J. Dong, W. Gao, Q. Han, Y. Wang, J. Qi, X. Yan, M. Sun, Plasmon-enhanced upconversion photoluminescence: mechanism and application. Rev. Phys. **4**(1), 100026–100062 (2019)
13. B. Shao, Z. Yang, J. Li, J. Yang, Y. Wang, J. Qiu, Z. Song, Upconversion emission enhancement by porous silver films with ultrabroad plasmon absorption. Opt. Mater. Express. **7**(4), 1188–1197 (2017)
14. H. Zhou, C. Wang, Y. Lai, J. Yu, S. Cheng, Plasmon-enhanced upconversion luminescence of the composite films through tunable ZnO spacer. Appl. Phys. A. **127**(5), 315–321 (2021)
15. E. Yablonovitch, T.J. Gmitter, Photonic band structure: The face-centered-cubic case. Phys. Rev. Lett. **63**(18), 1950–1953 (1989)
16. A. Mrabti, S. El-Jallal, G. Lévêque, A. Akjouj, Y. Pennec, B. Djafari-Rouhani, Combined photonic-plasmonic modes inside photonic crystal cavities. Plasmonics **10**(6), 1359–1366 (2015)
17. E.D. Martínez, A. Prado, M. Gonzalez, S. Anguiano, L. Tosi, L. Salazar Alarcon, H. Pstoriza, Integrating photoluminescent nanomaterials with photonic nanostructures. J. Lumin. **233**(9), 117870 (2021)
18. A. Das, K. Bae, W. Park, Enhancement of upconversion luminescence using photonic nanostructures. Nanophotonics **9**(6), 1359–1371 (2020)
19. Z. Yin, H. Li, W. Xu, S. Cui, D. Zhou, X. Chen, Y. Zhu, G. Qin, H. Song, Local field modulation induced three-order upconversion enhancement: combining surface plasmon effect and photonic crystal effect. Adv. Mater. **28**(13), 2518–2525 (2016)
20. G. Blasse, The physics of new luminescent materials. Mater. Chem. Phy. **16**(3–4), 201–236 (1987)
21. P. Ramasamy, P. Chandra, S. Rhee, J. Kim, Enhanced upconversion luminescence in $NaGdF_4$:Yb, Er nanocrystals by F^{e3}+ doping and their application in bioimaging. Nanoscale **5**(18), 8711–8717 (2013)

22. M. Xia, D. Zhou, Y. Yang, Z. Yang, J. Qiu, Synthesis of ultrasmall hexagonal $NaGdF_4$: $Yb^{3+}Er^{3+}$@$NaGdF_4$:Yb^{3+}@$NaGdF_4$:Nd^{3+} active-core/active-shell/active-shell nanoparticles with enhanced upconversion luminescence. Ecs. J. Solid. State. Sci. Technol. **6**(4), 41–46 (2017)
23. X. Zhang, B. Li, M. Jiang, L. Zhang, H. Ma, Core-spacer-shell structured $NaGdF_4$:Yb^{3+}/Er^{3+}@$NaGdF_4$@Ag nanoparticles for plasmon-enhanced upconversion luminescence. Rsc. Adv. **6**(43), 36528–36533 (2016)
24. Z. Lu, Z. Dan, G. De, Self-assembly $NaGdF_4$ nanoparticles: phase controlled synthesis, morphology evolution, and upconversion luminescence properties. Mater. Res. Express. **3**(2), 025009–025018 (2016)
25. P.A. Hiltner, I.M. Krieger, Diffraction of light by ordered suspensions. J. Phys. Chem. **73**(7), 2386–2389 (1969)
26. J. Liao, Z. Yang, S. Lai, B. Shao, J. Li, J. Qiu, Z. Song, Y. Yang, Upconversion emission enhancement of $NaYF_4$:Yb, Er nanoparticles by coupling silver nanoparticle plasmons and photonic crystal effects. J. Phys. Chem. C. **118**(31), 17992–17999 (2014)
27. S.A. Maier, H.A. Atwater, Plasmonics: localization and guiding of electromagnetic energy in metal/dielectric structures. J. Appl. Phys. **98**(1), 11101–11110 (2005)
28. V.N. Rai, A.K. Srivastava, C. Mukherjee, S.K. Deb, Localized surface plasmon resonance and refractive index sensitivity of vacuum-evaporated nanostructured gold thin films. Indian. J. Phys. **90**(1), 107–116 (2016)
29. H. Zhou, X. Wang, Y. Lai, S. Cheng, Q. Zheng, J. Yu, Upconversion improvement in $KLaF_4$:Yb^{3+}/Er^{3+} nanoparticles by doping Al^{3+} ions. Appl. Phys. A. **123**(10), 301–306 (2017)
30. P. Du, W. Ran, C. Wang, L. Luo, W. Li, Facile realization of boosted near-infrared-visible light driven photocatalytic activities of BiOF nanoparticles through simultaneously exploiting doping and upconversion strategy. Adv. Mater. Interfaces **8**(17), 2100749 (2021)
31. W. Park, D. Lu, S. Ahn, Plasmon enhancement of luminescence upconversion. Chem. Soc. Rev. **44**(10), 2940–2962 (2015)
32. L.A. Sweatlock, S.A. Maier, H.A. Atwater, Highly confined electromagnetic fields in arrays of strongly coupled Ag nanoparticles. Phys. Rev. B. **71**, 235408 (2005)
33. B.H. Bransden, C.J. Joachain, *Physics of atoms and molecules*, 2nd edn. (Addison-Wesley, Boston, 2003)
34. W. Xu, X. Chen, H. Song, Upconversion manipulation by local electromagnetic field. Nano Today **17**, 54–78 (2017)
35. V. Giannini, A.I. Fernández-Domínguez, S.C. Heck, S.A. Maier, Plasmonic nanoantennas: fundamentals and their use in controlling the radiative properties of nanoemitters. Chem. Rev. **111**(6), 3888–3912 (2011)
36. L. Liang, D.B.L. Teh, N.D. Dinh, W. Chen, Q. Chen, Y. Wu, S. Chowdhury, A. Yamanaka, T.C. Sum, C.H. Chen, Upconversion amplification through dielectric superlensing modulation. Nat. Commun. **10**(1), 1391 (2019)
37. D.N. Chigrin, D. Kumar, D. Cuma, G. von Plessen, Emission quenching of magnetic dipole transitions near a metal nanoparticle. ACS Photonics **3**(1), 27–34 (2016)